LHCb 2000-003 MUON
14 February 2000

Wire Pad Chamber for LHCb Muon System

B.Bochin, A.Kashshuk, V.Lazarev, N.Sagidova, E.Spiridenkov,
G.Velichko, An. Vorobiev, A. Vorobyov

Petersburg Nuclear Physics Institute

Abstract

Wire pad chambers (WPC) have been proposed for the outer Region 4 of the LHCb Muon System. These are double gap MWPCs with small wire spacing allowing to obtain 99% detection efficiency in a 20 ns time window. The chambers have a rectangular shape with the vertical dimension from 20 cm in Station 1 to 30 cm in Station 5. The horizontal dimensions will be different with the maximal size of 3 meters in Station 5. The wires are in the vertical direction. The short wire length allows to use small wire spacing needed for high time resolution. Also, this helps to obtain the uniform gas gain over the whole chamber area. The WPC has one row of the wire pads formed by grouping wires in separate readout channels.

Four WPC prototypes have been built at PNPI and tested in the PS beam at CERN. Here we report on the results from these tests. Also, the results of simulation of the WPC performance are presented.

1. Introduction

According to the LHCb Technical Proposal [1], the Cathode Pad Chambers (CPC) are considered as the candidates to be used in some areas of the Muon System. The first CPC prototype was constructed at PNPI and tested in the PS beam at CERN in November 1998. This was a single gap symmetric multi-wire proportional chamber with the following geometry parameters:

total gas gap - 5 *mm*,
wire spacing - 2 *mm*,
wire diameter - 25 μm,
wire length - 80 *cm*,
sensitive area - 30×80 cm^2.

One cathode plane contained pads of various sizes ranged from 1×2 cm^2 to 4×8 cm^2. The chamber operated with the $Ar/CO_2/CF_4$ gas mixture in various combinations of the components.

The front-end electronics was designed and produced at PNPI. Each channel contained a preamplifier followed by an amplifier-shaper. There were two outputs from each channel: *"fast"* with a 10 *ns* peaking time and *"slow"* with a 20 *ns* peaking time of the shaped signal. The fast signal was sent to a leading edge discriminator and then to a TDC. The slow signal was sent to a gated-ADC integrating the charge in a preset gate .

The results obtained with the pad sizes up to 32 cm^2 were encouraging: the time resolution was around 5 *ns* (*r.m.s.*) with ≈ 99% registration efficiency in a 25 *ns* time window. The chamber could operate with high rate beams (10^5 *particles/s·*cm^2). These results showed that with two planes of the CPCs one could obtain the registration efficiency ≥ 99% in a 20 *ns* time window which is the main requirement of the LHCb experiment.

The outer region (Region 4) of the LHCb Muon System contains pads with much larger sizes: from 4×20 cm^2 in Station 1 (M1) to 25×30 cm^2 in Station 5 (M5). The larger capacitances of these pads lead to deterioration of the time resolution. Therefore, the TP suggested subdivision of such pads into several pads of smaller sizes thus increasing considerably the number of the front-end channels.

The described below Wire Pad Chamber (WPC) was proposed with the goal to improve further the time resolution and efficiency of the chamber so it could operate with pads of larger sizes. Another goal was to make the chamber design as simple as possible with high redundancy and low cost so it could be used in Region 4 of all Stations (M1÷M5). The first prototype WPC –1 was

designed and constructed at PNPI and tested in the PS beam T11 at CERN in April/May 1999. These tests were continued in October/November 1999 with three new prototypes: WPC-1M, WPC-2, and WPC-3. Here we present the results obtained in these tests.

2. WPC design

If compared with the first CPC prototype, the design of the WPC prototypes contained some new features. Two gas gaps (5 *mm* each) and a smaller wire spacing (1.5 *mm*) should provide better efficiency and time resolution. The signals are taken from the wires that improves the signal-to-noise ratio thus allowing to work with larger pad sizes. The chambers have a rectangular shape with the sensitive area of 16×150 cm^2 (WPC-1 and WPC-3) and 16×24 cm^2 (WPC-1M and WPC-2). The wires are wound along the short side and grouped together to provide pads of various width with the constant length of 16 *cm*.

The short wire length has important advantages: it allows to reduce the wire spacing without introducing the additional wire support structure. Also, it becomes much easier to provide the constant gas gap along the wire length that results in high uniformity of the gas gain over the whole chamber surface.

Fig.1 shows a schematic view of the WPC prototypes. All the cathodes are made of 15 *mm* thick honeycomb panels with 1mm thick copper cladded FR4 plates glued to both sides of the panels. Such panels are industrially produced for the CMS Muon End Cap chambers, and the panels used to build the WPC prototypes were provided by the US/CMS collaboration. The anode wires of 30 μm in diameter were wound around the central cathode panel over 2.5 *mm* spacers glued along both sides of the panel. The continuous winding was performed using a winding machine that provided a permanent wire tension (30 *g*) and quite precise wire spacing (1500±40 μm) along the whole length of the chamber (1.5 *m*). The wire spacing precision was further improved to ±15 μm by placing temporary a high precision comb over the wires before they were glued with epoxy to the spacers. After that, all the wires were soldered to the strips on the anode bar placed at one edge of the panel. The length of the wire strips determined the size of the wire pads. The wires were cut at the ends of the strips.

Fig.2 shows the configuration of the wire pads in WPC-1 (pads $A_{1\text{-}8}$, $B_{1\text{-}8}$, $C_{1\text{-}8}$, $D_{1\text{-}8}$, $E_{1\text{-}4}$) . The pad size varies from 1×16 cm^2 to 8×16 cm^2. Note that the pad sizes of 4×16 cm^2 and 8×16 cm^2 are most interesting for Region 4 of the

Muon System. One side of each wire pad was connected to a common HV bus through a 2MΩ resistor. The other side of each pad was connected through a 1000 *pF* decoupling capacitor and a diode protection circuit to a preamplifier. All cathode planes were grounded in the WPC-1 prototype. The external plates were also grounded providing additional shielding of the chamber. The design of WPC-1M was identical. The difference was in the length of the chamber. WPC-1M contained only two 4×16 cm^2 and two 8×16 cm^2 wire pads (Fig.3).

The prototype WPC-2 contained four 2×16 cm^2 and four 4×16 cm^2 wire pads. In addition, the surface of the two cathode planes on external panels was subdivided into cathode pads as shown in Fig.4. There were two rows of pads (C_{iA} and C_{iB}) that could be readout from both sides of the chamber. Each two opposite pads from the two cathode planes were joined together into one readout channel. Such cathode pad structure is assumed to be in Region 3 of the Muon System. The prototype WPC-2 was designed specially for comparative study of the chamber performance in both WPC and CPC modes.

The prototype WPC-3 had the same sensitive area and wire pad structure as WPC-1. However, in addition to the wire pads, it contained also 1×150 cm^2 strips on the external cathode panels, the opposite strips being joined together into one readout channel.

All four prototypes contained similar wire pads, so they all could be used to study the chamber performance in the WPC mode. In this report, we consider only the results obtained with the wire pads, thus limiting ourselves by consideration just Region 4 in Stations M1÷M5. Note, however, that this region covers 75% of the whole area of the Muon System.

3. Electronics

The WPC prototypes were equipped with the front-end electronics that was used in the previous tests of CPC-1. This electronics, based on discrete elements, was designed and constructed at PNPI. The WPC-2 prototype allowed also the replacement the PNPI FE electronics by the FE electronics based on the SONY-chip [2] in both the cathode and the anode channels. This made it possible to perform a comparison of these two types of FE electronics. The results will be presented in a separate report. As it was mentioned above, each channel of the PNPI FE electronics contained a fast (F) and a slow (S) outputs. The signal shaping was optimised for detection of the chamber current with the following time dependence:

$$I(t) \propto \frac{Q_0}{t + t_0} \qquad (1)$$

where Q_o is the total charge of the avalanche created by a single ionization electron. The parameter t_o was taken to be equal to 1.87 *ns*. The shaper contains four stages. The first one transfers the signal shape of the ~ *1/t* type into an exponent. Then the signal is integrated with three identical RC-chains operating independently. The difference between the F-channel and the S-channel is only in the value of the time constants of the integration with RC-chains. It is 2.1ns in the F-channel and 6.3ns in the S-channel. The input resistance of the preamplifier is 30Ω plus a 20Ω contribution of the external diode protection circuit. The calculated sensitivities of the channels and the equivalent noise charge (ENC) are as follows:

$$\text{Sensitivity } (\textit{F-channel}) = \begin{cases} 5\ mV/fC & \text{at } C_{in} = 50\ pF \\ 2.5\ mV/fC & \text{at } C_{in} = 200\ pF\ ; \end{cases}$$

$$\text{Sensitivity } (\textit{S-channel}) = \begin{cases} 2\ mV/fC & \text{at } C_{in} = 50\ pF \\ 1.5\ mV/fC & \text{at } C_{in} = 200\ pF\ ; \end{cases}$$

$$\sigma_n\,(\textit{F-channel}) = 1250e + 50\ e/pF,$$
$$\sigma_n\,(\textit{S-channel}) = 1870e + 20\ e/pF.$$

Here, C_{in} are the total input capacitances. In the constructed WPC prototypes, C_{in} were measured to be:

$C_{in} \approx 65\ pF$ ($2\times16\ cm^2$ pad),
$C_{in} \approx 110\ pF$ ($4\times16\ cm^2$ pad),
$C_{in} \approx 200\ pF$ ($8\times16\ cm^2$ pad).

The measured sensitivity and the noise level proved to be in agreement with the calculated values.

Fig.5*a* presents the calculated response of the amplifier-shaper in the F-channel to a δ–signal. One can see that the output signal reaches its peak value in 10 *ns* after sending of the δ–signal at the input. Note, however, that the rise time from 10% to 90% of the output signal is only ≈4 *ns*. The calculated shape of the 'real' signal produced by a single ionization electron is shown in Fig.5 *b*.

In this case the amplitude of the output signal is reduced by a factor of ≈10 and the peak time is increased up to 15 *ns* with the rise time about 7 *ns*.

4. Simulation of WPC performance

Simulation of the WPC performance has been done using the program developed at PNPI. Some details of the simulation program can be found in the LHCb Note [3] describing performance of the Micro-Cathode-Strip chambers (MCSC) which has much in common with the WPC in the part concerning the time resolution of the chamber. Here we present only some concluding results of the WPC simulation.

Fig.6 presents the electric field map in WPC. It was assumed that the chamber is filled with the Ar(60%)+CO_2(30%)+ CF_4(10%) gas mixture with the high voltage HV=2700V. At this high voltage the gas gain is expected to be 1.2×10^5 according to the previous measurements with this gas mixture (see chapter 5.3).

The simulation program starts with the distribution of the ionization electrons along the particle trajectory, then it considers the drift of the ionization electrons towards the anode wires taking into account the diffusion and the attachment of the ionization electrons to electro-negative gases (CF_4 in our case). Then it calculates the avalanches produced by the ionization electrons. Finally, it calculates the time development of the charges induced on the cathode pads and on the anode wires and provides the signals at the outputs of the readout channels. The signal shaping and the amplification in the readout channels were adjusted as in the real readout electronics in our measurements. It was accepted that the noise level in the fast channel was 4 *mV* (*r.m.s.*) and the input resistance was 40 Ω. Note that in this analysis the double gap WPC was considered as two independent single gap chambers with well controllable wire staggering of one chamber with respect to another. The time distributions of the signals exceeding a preset threshold in each chamber were calculated, and the overall time distribution was determined as a convolution of the two spectra. Then the detection efficiency was found in various time windows: 25 *ns*, 20 *ns*, and 15 *ns*.

The calculation were performed for 9 *GeV/c* pions entering the chamber perpendicular to its surface with a variable coordinate *Y* along the axis in the wire plane perpendicular to the wire direction. The calculated mean number of the ionization electrons along the pion track in the 5mm gap was 47.3. The electric field in the drift space is about 7 *kV/cm* (Fig.6). This corresponds to the

electron drift velocity of 80 *μm/ns* (Fig.7*a*) and to the total collection time of the electrons around 30 *ns*.

One uncertainty in the simulation is related to unknown attachment probability of the electrons. According to the Magboltz program [3], this probability is quite high in the $Ar/CO_2/CF_4$ gas mixture due to presence of CF_4, especially in the region around the anode wire where the electric field exceeds $E \approx 20$kV/cm (Fig.7*b*). Therefore, an essential part (40% in our case) of the ionization electrons could be lost before they create the avalanches. Unfortunately, there are no direct measurements of this probability so far.

The gas amplification factor $\alpha(E)$ was calculated using the following expression:

$$\alpha(E) = A \times \exp(\frac{-B}{E}) \qquad (2)$$

Here E is the electric field in V/cm. Parameters A and B were found from a fit to the $\alpha(E)$ calculated with the Magboltz program in the region $E \leq 100$ kV/cm: $A=12480$, $B=1.41\times10^5$ V/cm. Thus obtained expression (2) was used also to calculate $\alpha(E)$ at $E > 100$.

With the attachment coefficient $\eta(E)$ given in Fig.7*b* and with $\alpha(E)$ determined by (2), the calculated signals proved to be much higher than those observed in the experiment. The agreement could be achieved after renormalization of $\alpha(E)$:

$$\alpha^* = K_\alpha \times \alpha(E), \; K_\alpha = 0.7 \qquad (3)$$

Fig.8 demonstrates the calculated time distribution of the signals in a single gap WPC produced by the ionizing particles (9 *GeV/c* π-mesons) entering the chamber perpendicular to the chamber plane $(\Theta = \varphi = 0)$ and crossing the anode wire plane at different distances from the wire: *Y/S*=0; 0.2; 0.4; 0.5. Here *S* is the wire spacing and *Y/S* is the shortest distance of the trajectory from the anode wire.

One can see some delay of the first arrivals of the electrons on the anode wires with increase of *Y/S*. The maximum delay is 10 *ns* at *Y/S*=0.5. However, the probability to find the signal beyond the 25 *ns* window (that is beyond 30 *ns* after the particle arrival time) remains small for any *Y/S* value. Therefore, one should not expect any strong dependence of the time resolution and the efficiency of the double gap WPC on the staggering of the anode wires. This statement is illustrated in Fig.9. It shows the calculated time resolution and

inefficiency of the double gap WPC for various staggering of the anode wire planes. Such small dependence of the double gap WPC behavior on the staggering of the anode wire planes is a valuable feature of this chamber. Otherwise, it would be difficult to keep the proper staggering in the all areas of the Muon System with different inclinations of the incoming particles.

Fig.9 shows also the dependence of the time resolution and efficiency on the discriminator thresholds. Decreasing of the threshold from 30 *mV* to 20 *mV* leads to a noticeable improvement of the WPC performance. Note, that the 20 *mV* threshold proved to be achievable in the real conditions of the beam tests even in the presence of some pickup noise in the experimental area.

Fig.10 presents the calculated WPC inefficiency in various time windows for staggering δ/S=0.5. As it follows from these calculations one can reach 99.8%, 99.3%, and 97% efficiency in the time windows 25 *ns*, 20 *ns*, and 15 *ns*, respectively, with the double gap WPC operating with the gas gain of 1.2×10^5.

5. Beam tests

5.1 Experimental setup

All the WPC prototypes have been tested at CERN in a 3 *GeV/c* negative pion beam at PS.

The layout of the experiment is shown in Fig.11. Beam particles were detected with two scintillator counters: S1 (*15cmx15cm*) and S2 (*20cmx20cm*). The coincidence between these two counters in a 10 *ns* window provided a trigger signal:

$$TR1 = S1 \& S2$$

The constant-fraction discriminators (CFD) was used in both *S1* and *S2* channels helping to reduce the time jitter of the trigger signal down to ≤1ns. The beam particles were detected also by two planes (*H*-horizontal and *V*-vertical) of the hodoscope counters, each plane containing 8 counters (1*cm*×8*cm*). The following information was registered by the acquisition system:

- Time arrivals and amplitudes of the signals from S1 and S2 measured with TDCs and ADCs;
- Time arrivals of the signals from all hodoscope counters measured with TDCs;
- Time arrivals of the signals from the WPC F-channels;

- Integrated current signals from the WPC S-channels.

The signals from the WPC F-channels were sent to leading edge discriminators (Le Croy 4416B) with adjusted thresholds, and the output signals from the discriminators were registered with 16-bit TDCs (Le Croy 1176). The common stop TDCs were stopped by *TR1* signal and allowed to measure the time intervals of 64 μs before the stop. The 14-bit ADCs (Le Croy 1182) gated by the *TR1* signal integrated the current signal in the 80 *ns* time window.

In addition, there was ungated data from the scalers detecting signals from all scintillator counters and from the WPC F-channels. The scalers provided two types of information: the total number of counts during the beam spill and the number of counts during a 1 *sec* interval in-between the beam spills. The beam spill was around 330 *ms*.

5.2 Off-line event selection

The main results of the data analysis are the ADC and TDC spectra of the signals from the WPC S-channels and F-channels, respectively. The events were selected after several cuts applied to the raw data from the beam defining scintillator counters and the hodoscope:

- *Cut1. Shower rejection*.
  - Large amplitudes in the ADC spectra from the S1 and S2 counters were rejected. The pile-ups of two and more particles in a 20 *ns* time window were rejected in this way. Typically, about 10% of the events were rejected by this cut. The remaining events were considered as *TR2*-events.
- *Cut2. Hodoscope selection.*
  - Only signals in a 20ns time window in the TDC spectra were selected.
  - There should be one and only one signal both in the H-plane and in the V-plane of the Hodoscope. This helps to kill further the showers in the beam.
  - A certain combination of the hodoscope counters could be selected to define a beam spot.

The events passing *Cut1* and *Cut2* were considered as *TR3*-events. No cuts have been applied to the signals from WPC.

The number of the *TR3*-events was used in calculations of the efficiencies in the WPC S-channel and F-channel:

$$Eff_{ADC} = \frac{\sum_{i=300}^{overflow} N_{i(ADC)}}{\sum TR3} \qquad (5)$$

$$Eff_{TDC} = \frac{\sum_{t1}^{t1+\Delta t} N_{i(TDC)}}{\sum TR3} \qquad (6)$$

As an example, Fig.12 shows the ADC and TDC spectra of the signals from a wire pad (W_3 of 4×16 cm^2 size) of the WPC-2 prototype. The measurements have been performed with the Ar(40%)+CO_2(45%)+ CF_4(15%) gas mixture at HV=3.15 kV corresponding to the gas gain of $2 \cdot 10^5$. The beam spot was selected to be inside the W_3 pad. The pedestal in the ADC spectrum is positioned in the channel 250 with a spread of 12 channels (*r.m.s.*) caused by the electronics noise. The empty space in the region below the channel 500 demonstrates high efficiency in the ADC-channel. Quantitatively, Eff_{ADC}=99.9%

The time resolution in the TDC channel was found to be 2.9 *ns* (*r.m.s.*) with the efficiency of 99.8%, 99.7%, and 98.8% in the time windows of 25 *ns*, 20 *ns*, and 15 *ns*, respectively. These results are in agreement with predictions followed from our simulation studies.

5.3 Gas gain calibration

The absolute gas gain was measured by an ATLAS group at BNL with a wire chamber having the same wire diameter, d_a=30μm, as in our WPC. They used an Ar(60%)+CO_2(30%)+ CF_4(10%) gas mixture and obtained the gas gain of 1.2×10^5 at the electric field on the anode wire surface *Ea*=225kV/cm.

Note that the gas gain (*G*) is defined here as the ratio of the total charge Q_{tot} collected by the anode wire to the total number of ionization electrons Q_i created by the incident particles:

$$G = \frac{Q_{tot}}{Q_i} \qquad \mathbf{(7)}$$

This definition ignores the fact that some part of the ionization electrons may disappear due to attachment to the electronegative molecules without producing the avalanches. To be comparable with the BNL results, we performed measurements with the same gas mixture. The similar electric field on the anode wire surface *Ea*=225kV/cm is reached in WPC at HV=2.7kV (Fig.6). Therefore, the gas gain of 1.2×10^5 is expected at HV=2.7kV in WPC filled with the BNL gas mixture. Fig.13 shows the HV dependence of the mean charge determined from the ADC spectra (*ADC_mean*) for various wire pads. One can see from this figure that at HV=2.7kV the *ADC_mean* is around channel 1000 for 2x16 cm^2 and 4×16 cm^2 pads and around channel 900 for the largest pad of 8×16 cm^2 size. We used these values for normalization of the gas gains measured with other gas mixtures.

5.4 Gas gain in various gas mixtures

The $Ar/CO_2/CF_4$ gas mixture is considered at present as the best choice for the wire cathode strip chambers used in the CMS and ATLAS Muon Systems. This mixture provides fast collection of the ionization electrons (due to CO_2 and CF_4), very good ageing properties (due to CF_4), and relatively low high voltage (due to Ar). All these features are attractive also for application of this gas mixture in the LHCb muon chambers where the time resolution and the ageing properties are of primary importance. We have studied the $Ar/CO_2/CF_4$ gas mixtures with the goal to find the ratio of the components optimal for the LHCb muon chambers.

Fig.14 presents the HV-dependence of the measured gas gain in various $Ar/CO_2/CF_4$ gas mixtures. One can see that the gas gain depends strongly on the amount of Ar but it is not so sensitive to the replacement of CO_2 by CF_4. With increase of the high voltage, the gas gain is increasing up to a maximum value around 4×10^5 (nearly the same in all studied gas mixtures) where the sparks and dark current start to appear.

We investigated also the gas mixture with CF_4 replaced by $C_2H_2F_4$ (freon). This freon is widely used now in RPCs and other devices showing high stability against sparking. The results are presented in Fig.15 demonstrating the current produced by the beam in WPC as function of the high voltage. Note that the current around $1\mu A$ corresponds to the gas gain of 2×10^5. One can see from Fig.15 that the gas gain as high as 10^6 can be reached with the $Ar(40\%)+CO_2(45\%)+ C_2H_2F_4(15\%)$ gas mixture. The chamber shows stable operation up to HV=3.6kV. The trips have been observed only at HV=3.7kV

with immediate recovery after the trip. This allows, for example, to operate WPC with the gas gain up to 4×10^5 (HV=3.4*kV*) with a sufficient plateau before the instability region. Such regime might be recommended for Region 4 of the Muon System where the ageing limitations could allow WPC operation with such gas gains.

Comparison of the ADC spectra showed that the replacement of 15% CF_4 by 15% of $C_2H_2F_4$ reduces the pulse height by a factor of 1.7. To restore the pulse height one should increase HV by ≈100V (see Table 3).

5.5 Time resolution

The high time resolution of the muon chambers is one of the main requirements of the LHCb experiment. In fact, it is required that the detection efficiency of each Muon station should be ≥ 99% in the 20 *ns* time window. Assuming that each station contains two layers of the muon chambers, this requirement could be well satisfied if each layer provides ≥ 95% efficiency in the 20 *ns* time window. In terms of the time resolution of the muon chambers this means that the *r.m.s.* of the time distributions should be less than 5 *ns*.

In order to select the gas mixture, we compared the time resolutions measured with various $Ar/CO_2/CF_4$ gas mixtures in identical conditions: the same beam focused on the same pad at the same gas gain. The results are presented in Table 2. The measurements were performed at the gas gain of 1.2×10^5 with a 4×16 cm^2 pad size. The beam was perpendicular to the chamber plane.

Table2.
Time resolution of WPC with various $Ar/CO_2/CF_4$ gas mixtures.
WPC-1 prototype.
The wire pad size is $4\times16cm^2$. Data corresponds to the same gas gain of 1.2×10^5.

Gas mixture $Ar/CO_2/CF_4$	Time resolution, *r.m.s.* *(ns)*
40/40/20	3.04
40/45/15	3.07
40/50/10	3.20
40/55/5	3.27
60/30/10	3.49
30/60/10	3.13

The comparison shows that the time resolution with the gas mixture containing 60% of Ar is noticeable worse (by 0.4 *ns*). The time resolution with the other gas mixtures is not much different, though with some preference to the larger CF_4 concentration. The disadvantage of the 30/60/10 gas mixture is the higher voltage required to get the same gas gain. So our choice was the $Ar(40\%)+CF_4(x)+CO_2(60\%-x)$ gas mixture where x=10, 15, or 20%.

We made also comparison of the time resolution obtained with the $Ar(40\%)+CO_2(45\%)+C_2H_2F_4(15\%)$ and $Ar(40\%)+CO_2(45\%)+CF_4(15\%)$ gas mixtures. The measurements have been performed with the larger pad size of 8×16 cm^2. Table 3 demonstrates the results of this comparison. One can see that the time resolution of WPC is the same (or slightly better) when CF_4 is replaced by $C_2H_2F_4$ and HV is increased by ~100V to restore the signal amplitude. However, the chamber can operate in this case at much higher HV with considerably improved time resolution (see also Fig.16). As an example, Fig.17 demonstrates the ADC and TDC spectra measured with the WPC-1M prototype at HV=3.45 kV. One can see that the time resolution becomes better than 3 *ns* (*r.m.s.*) even operating with the large pads of 8×16 size. This consideration shows a clear advantage of the freon containing gas mixture, especially if the experimental conditions allow the chamber operation at high gas gains in the region of 4×10^5 .

Fig. 18 presents the time resolution and the time walk in function of the signal amplitude. For this purpose, the ADC spectrum similar to that shown in Fig. 12 was subdivided in 5 zones. The time resolution (*TDC_r.m.s.*) and the peak position in the TDC spectrum (*TDC_ mean*) were determined for each zone.

One can see that the time resolution is saturated on a level of *r.m.s.*=2.8 *ns* at the signal amplitudes ≥ 1500ch ADC. The essential deterioration of the time resolution (*r.m.s* = 3.8 *ns*) is observed only in zone 1 ($500\leq Q\leq 1000$ch). However, this zone contains only 5% of the ADC spectrum. The total time walk is 6 *ns* (*TDC_ mean*), but the time walk in the most populated regions 2, 3, and 4 (85% of the events) is only 2 *ns*.

Our simulation studies showed that the time resolution of the double gap WPC should not depend strongly on the wire planes staggering and thus on the beam inclination. The experiment showed that this expectation is correct.

Fig. 19*a* presents the measured HV-dependence of the time resolution (*r.m.s.*) for various θ-angles *(θ=0°, 100 mrad, and 200 mrad)*. Here θ is the

chamber rotation angle around the wire direction. One can see that the time resolution proved to be practically independent on the θ-angle in the measured θ-range.

Table 3.
Time resolution of WPC with Ar(40%)+CO_2(45%)+ CF_4(15%) and Ar(40%)+CO_2(45%)+ $C_2H_2F_4$(15%) gas mixtures.
The measurements were performed with a 8×16cm^2 wire pad.

Ar(40%)+CO_2(45%)+ CF_4(15%)

HV (kV)	3.05	3.1	3.15	3.20	3.25	3.3
ADC mean (*ch.*)	1190	1430	1720*	2075	2425	
TDC r.m.s. (*ns*)	5.0	4.33	3.95	3.5	3.3	

Ar(40%)+CO_2(45%)+ $C_2H_2F_4$(15%)

HV (kV)	3.15	3.20	3.25	3.30	3.35	3.4	3.45	3.5	3.55	3.60	3.65
ADC mean (*ch.*)	1217	1394	1654	1959	2343	** 2621	** 2903	** 3210	over	Over	
TDC r.m.s. (*ns*)	4.73	4.32	3.93	3.48	3.22	3.16	2.9	2.8			

**) This "ADC_mean" corresponds to the gas gain of 2×10^5;*
***) The numbers are underestimated due to ADC overflow (>4000 ch).*
The shaded areas correspond to the end of the regions of the WPC stable operation.

5.6 Detection efficiency

Fig.19*b* shows the HV-dependence of the detection efficiency in a 25 *ns* window in the TDC spectra measured with the WPC-1 prototype at various θ-angles. The measurements were performed with the Ar(40%) + CO_2 (50%) + CF_4(10%) gas mixture. The wire pad size was 4×16 cm^2, the discriminator threshold was set at 20 *mV*. The particles were selected with the hodoscope to be inside the pad size.

One can see that the efficiency is close to 100% with the plateau from HV=3.0 kV (θ = *0°*) or from HV=2.95 kV (θ = *100 mrad and 200 mrad*) to HV=3.25 kV. Note that the gas gain is 1×10^5 at HV=3.0 kV and 2×10^5 at HV=3.15 kV. Comparison with Fig.19*a* shows strong correlation between the time resolution and the efficiency: the efficiency in a 25 *ns* window becomes better than 99% when *r.m.s.*≤5 *ns*.

Table 4 presents the results of the measurements of the detection efficiency for high beam intensities. It is expected that the LHCb muon chambers should operate at high counting rates up to 300 kHz per channel.

Table 4. *WPC efficiency measured at various beam intensities.*

Counting rate per channel		Eff_{TDC}/ Eff_{ADC}			
	Eff_{ADC}	30 *ns*	25 *ns*	20 *ns*	15 *ns*
κHz	*%*	*%*	*%*	*%*	*%*
54	99.68	99.9	99.85	99.8	98.5
117	99.52	100.0	99.95	99.95	99.0
255	99.54	99.93	99.83	99.6	98.5
365	99.43	99.95	99.95	99.9	98.5
420	99.42	99.8	99.7	99.6	98.0
510	99.46	99.8	99.8	99.6	97.5
700	98.22	99.75	99.7	99.6	97.9

The measurements were performed with the WPC-1 prototype with the Ar(40%) +CO_2(40%)+CF_4(20%) gas mixture. The high voltage was HV=3.15 *kV* corresponding to the gas gain of $2 \cdot 10^5$. The wire pad size was 4×16 cm^2. The beam spot was selected by hodoscope to be inside the pad size. The beam density was varied from 4.5 *kHz/cm²* to 100 *kHz/cm²*. At the same time the beam intensity (*S1&S2* coincidences) was varied from 84 *kHz* to 1.1 *MHz* and the counting rate in the pad channel was varied from 54 *kHz* to 700 *kHz*.

The Eff_{ADC} was determined according to eq. (5). In spite of the hodoscope selection, approximately 1% of the particles were detected by the neighbor pads, and they were subtracted from the number of *TR3*-events when calculating the Eff_{ADC}. To exclude the influence of the missing particles, the Eff_{TDC} was calculated as the ratio of the number of the events in the TDC window (30 *ns*, 25 *ns*, 20 *ns*, or 15 *ns*) to that detected in the ADC channel (>350ch). One can see from Table 4 that the Eff_{TDC} in 20 *ns* window remains higher than 99.5% even at the highest beam intensity.

However, we should note here that thus obtained efficiency may be overestimated as the dead time introduced by the signal width in the WPC F-channel can be shadowed by a 80 *ns* dead time in the *TR1* circuit.

5.7 OR-signal efficiency

The maximal size of the physical pad is determined by two factors. One is the pad capacitance value that deteriorates the time resolution. The other one is maximal admittable occupancy per pad. The effect of large capacitance is illustrated by Fig.20 showing Eff_{TDC} in a 25 *ns* window vs high voltage measured with two different pad sizes - 4×16 cm^2 and 8×16 cm^2. One can see that the plateau for the 8×16 cm^2 pad is reduced by ≈100V that is not acceptable if we do not want to operate the chamber with the gas gain exceeding 2×10^5. However, one can separate the large pad into two or more smaller pads with separate FE electronics and join them by a logical OR after the discriminators. We have tested this procedure with the goal to see the resulted time resolution and efficiency. The experiment was performed with the WPC-1M prototype. The beam was centered in-between the W3 and W4 pads with the sizes of 4×16 cm^2 each. The gas mixture was Ar(40%)+CO_2(45%)+CF_4(15%). The signals from the outputs of the discriminators in the W3 and W4 were ORed and sent to a TDC. The measured efficiency in the 25 *ns* window is presented in Fig.20. One can see

from this figure that the OR-efficiency of the two 4×16 cm^2 pads is exactly the same as the efficiency of one 4×16 cm^2 pad channel. That proves that the OR-procedure does not spoil the time resolution. This conclusion was also checked in the beam intensity scan. It was shown that the OR-efficiency in the 20 *ns* window remains above 99% at the counting rate of 500 *kHz* per channel (1 *MHz* beam intensity). The above consideration justifies the proposal to arrange the logical X- and Y-strips by combining in OR the appropriate number of physical pads and to use these strips as a large-size logical pads. This leads to a considerable reduction in the number of logical pads and, as a consequence, to essential reduction in the cost of the electronics.

5.7 Cross-talks

The probability to fire the neighbour and non-neighbour wire pads was investigated with the WPC-1 prototype. The gas mixture was Ar(40%)+CO_2(40%)+CF_4(20%). The high voltage was HV=3.15kV; the gas gain 2×10^5; the discriminator threshold was 20 *mV*. The beam spot was centered on the W_{C2} pad of 8×16 cm^2 size. The neighbour pads were W_{C1} (8×16 cm^2) and W_{C3} (4×16 cm^2).

The selection procedure described in section 5.2 has allowed to reject the major part of the showers in the beam that is very important in the cross-talk studies. The remaining showers were eliminated by signals with large amplitudes (>800 channel ADC) arriving in the same time interval as the signals in the W_{C2} pad. Such large-amplitude events (2% of the total statistics) could not be the result of the cross-talk. After that the probability to find a hit in a 30ns TDC time window in coincidence with a similar hit in W_{C2} was determined. 15000 events have been analysed with the following results:

Hit only on W_{C2} 98%;
Hit on W_{C2}&W_{C1} 1.2%;
Hit on W_{C2}&W_{C3} 1.1%;
Hit on W_{C2}&W_{C1}&W_{C3} 0.6%;
Hit on W_{C2}&OR on 11 non-neighbour pads 0.25% .

More detailed information was obtained by subdividing the ADC spectrum on W_{C2} in 5 zones and considering the cross-talk dependence on the signal amplitude on W_{C2}. The results are presented in Fig.21. One can see that the cross-talk is very small for all signal amplitudes except the overflow

zone 5. It did not exceed 0.1% even on neighbour pads. But it is about 10% for the overflow signals, most of the cross-talk signals on W_{C1} and W_{C2} being strongly correlated. Such behaviour is explained in Fig.21. It shows the observed shifts of the pedestals on the pads in coincidence with the signals on W_{C2}. One can see that the shift is maximal on the neighbour pads and it is proportional to the signal amplitude on W_{C2}.This shift is explained by the pad-to-pad capacitance coupling. At some signal level on W_{C2} , the shift is approaching the discriminator threshold, thus producing the cross-talk signal. This picture agrees with direct observation of the signals in the scope showing that the amplitude of the cross-talk signal on the neighbour pad is around 2% of the signal amplitude on the fired pad. Anyhow, the total cross-talk is quite small as it was expected for such design of the chamber.

6. Ageing

Detailed ageing studies of the wire chambers with the $Ar/CO_2/CF_4$ gas mixture have been performed at PNPI in the frame-work of the CMS End Cap Muon System programme [4]. One should stress that the WPC/CPC chambers are made precisely from the same materials as the CMS chambers and use the same gas mixture. Therefore, the results obtained for the CMS chambers are directly applicable to the WPC/CPC chambers proposed for the LHCb Muon System. These tests showed that with the gas mixtures $Ar/CO_2/CF_4$ in the relative proportions 30/50/20 as well as 40/50/10 the deterioration of the chamber performance (gas gain and the dark currents) was not obseved up to the accumulated charges of 13 *C/cm wire*.

The global irradiation tests of the CMS chambers have been started last year at GIF facility at CERN. So far only a modest charge has been a collected (0.2 *C/cm wire*), but the tests will be continued in March/April 2000. Allowing a limit for the accumulated charge of 1 *C/cm wire,* one can calculate that the WPC/CPC chambers with the $Ar/CO_2/CF_4$ gas mixture operating at the gas gain of $\approx 2\times10^5$ satisfy the ageing requirement over the whole Muon System accept region 1 and region 2 in Station M1. As concerns Regions 3 and 4 , the gas gain could be considerably increased in these stations. Therefore, the $Ar/CO_2/C_2H_2F_4$ gas mixture seems very attractive as it allows safe WPC operation at high gas gains. Unfortunately, the ageing properties of this gas mixture are unknown at present. We are planning to perform the local ageing tests at PNPI with the $Ar/CO_2/C_2H_2F_4$ gas mixtures using a WPC prototype. These tests will be started

in March 2000. Also, global ageing tests of the WPC filled with the $Ar/CO_2/C_2H_2F_4$ gas mixture are planned to be performed at GIF in March/April 2000 in parallel with the CMS tests. These tests will show whether the $Ar/CO_2/C_2H_2F_4$ gas mixture could be used only in the outer regions of the Muon System or it can be used also in the inner regions (with smaller gas gains) providing much larger plateau and thus increasing the redundancy of the Muon System.

7. Construction and cost

The WPC chambers are designed to make their construction as simple as possible. The wires are wound along the short side of the chamber that make it possible to use the small wire spacing (1.5mm) needed for good time resolution without additional wire support structure. There is no severe requirement to the flatness of the cathode plane to be produced in industry.

The cost of materials in the double gap WPCs is estimated to be around 1000 CHF per 1 m^2 of chambers. The WPCs are proposed to be used in region 4 of all Muon stations covering 75% of the total area of the Muon System, that is about 325 m^2. With two layers in each station, this gives 650 m^2. The chamber sizes will vary from 20×190 cm^2 in station M1 to 30×300 cm^2 in station M5. Each station will contain 96 chambers per layer. In total, there will be 960 chambers in Region 4 of the whole Muon System.

The two layer structure of the Muon stations allows to arrange a simple overlapping in both X and Y directions leaving no dead zones in the whole area. The design of the CPCs in Region 3 being very similar with to the WPC design, there will be no problem in overlapping Region 3 and Region 4.

8. Conclusions

Four WPC prototypes have been constructed at PNPI and tested in the PS beam at CERN. The performance of these prototypes proved to be in agreement with the expectations followed from the simulation study. Most of the measurements were performed with the $Ar/CO_2/CF_4$ gas mixture which provides fast collection of the ionization electrons and has very good ageing properties. Also, a new $Ar/CO_2/C_2H_2F_4$ gas mixture has been tested with remarkable results: this mixture proved to be as fast as the $Ar/CO_2/CF_4$ mixture. However, it is much more stable against discharges that allowed to extend the plateau by additional 300 *V* and to operate the chamber with the gas gains up to 4×10^5. The

ageing properties of this new gas mixture will be studied in the near future. We do not expect any problems in Region 4 of the Muon System where the ageing requirements are not so strong: the charge accumulated by the wires will not exceed 0.1 *C/cm wire* during 10 LHC years even at the gas gain of $(4\div5)\times10^5$. The ageing tests will show if this gas mixture could be used also in the inner regions of the Muon System.

The results obtained in the beam tests can be shortly summarised as follows:

- The detection efficiency in a double gap WPC with the wire pad sizes up to 64 cm^2 proved to be better than 99% (25 *ns* window) with a 300 *V* plateau in the case of the $Ar/CO_2/CF_4$ gas mixture and with a 550 *V* plateau in the case of the $Ar/CO_2/C_2H_2F_4$ gas mixture. Within this plateau, the gas gain varies from 8×10^4 up to 3×10^5 (CF_4 , HV=3.25 *kV*) or up to 1×10^6 ($C_2H_2F_4$, HV=3.6 *kV*), and the time resolution varies from 4.7 *ns* (*r.m.s.*) to 2.8 *ns* with about 3 *ns* in the middle of the plateau.
- The higher gas gain attainable with the $Ar/CO_2/C_2H_2F_4$ gas mixture allows to use wire pads of much larger sizes. In particular, it was demonstrated that 99% efficiency in a 25 *ns* window is reached within a 400 *V* plateau with the pad size of 128 cm^2. The gas gain is 4×10^5 in the middle of the plateau at HV= 3.4 *kV*.
- The time resolution and the efficiency remain practically unchanged up to the rates of 500 *kHz* per channel. (Note, however, a comment in the text about the dead time introduced by the beam trigger).
- The cross-talks are quite low. The probability to fire the neigbouring pads is about 2%. The cross-talks with the non-neighbour pads are negligible.

The detection efficiency required for each muon station is 99% for 20 *ns* time window. The above consideration shows that this requirement is practically satisfied already with one WPC layer. With two WPC layers, the Muon System will have a strong enough redundancy. Also, the two-layer structure of the muon stations and the uniform technology in all regions allow to construct the Muon System without any dead zones.

One should mention also some other advantages of the WPC technology:

- Projectivity of pad sizes in the non-bending (Y) plane;
- Flexibility of the pad sizes in the bending (X) plane;
- Possibility to combine pads in OR into logical strips of various sizes without deterioration the time resolution;

- Non-flammable gas mixture with very good ageing properties proved experimentally with the $Ar/CO_2/CF_4$ gas mixture. To be checked with the $Ar/CO_2/C_2H_2F_4$ gas mixture.

One should point out that the presented here results were obtained with the PNPI FE electronics specially designed for this chamber. This electronics is made with discrete components. The next step is to find the appropriate FE chip that could provide a similar performance. There are several candidates for such chip, and the tests of these chips are on the way.

Acknowledgements

The authors would like to express their gratitude to the LHCb muon group helping in preparations and performing the beam tests at CERN. In particularly, we are thankful to the CERN group with B.Schmidt, R.Lindner, T.Schneider, J.Lamas Valverde and G.Corti who provided the data acquisition and beam trigger systems, the gas supply lines, and other equipment needed in the test run. We would like to thank G.Carboni and his group from Rome II providing the hodoscope and also we would like to thank L. de Paula, M.Gandelman, E.Polycarpo and D.Moraes from UFRJ participating in the data taking and in the data analysis. Many thanks to B.Schmidt and to W.Riegler for numerous and valuable discussions, and to H.J.Hilke for discussions and for financial support of this work.

References

1.LHCb Technical Proposal. CERN/LHCC 98-4, LHCC/P4, 20 February 1998.

2.O.Sasaki. ATLAS Internal Note, 1 Osctober 1999.

3.G.Velitchko. LHCb Internal Note 98-016, 2 February 1998.

4. CMS Note 1999/011.

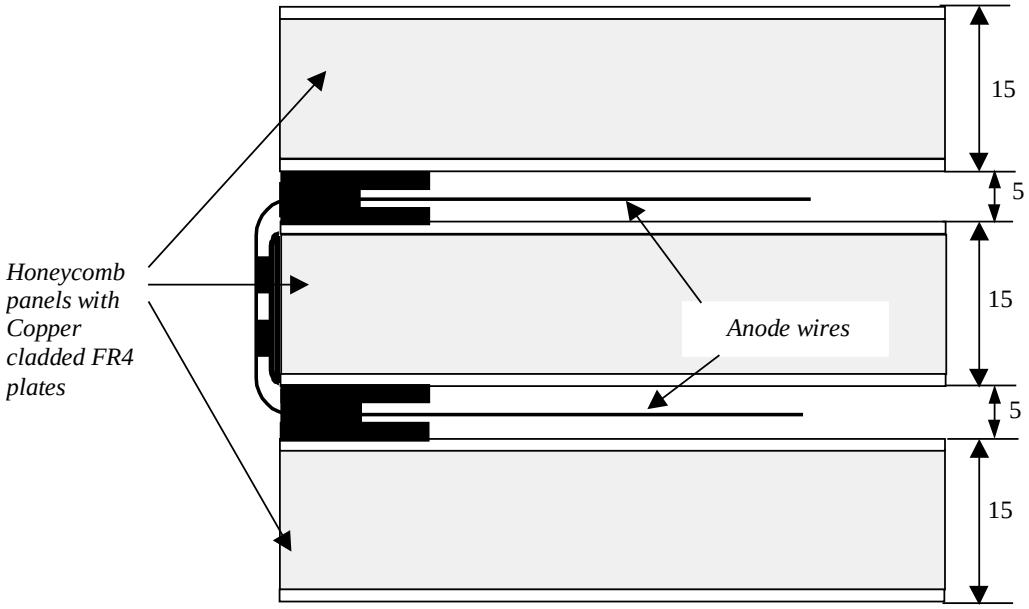

Fig.1. Cross-section view of WPC prototypes.

Dimensions are in mm, wire spacing is 1.5mm, the wire diameter is 30 μm, the wire length is 16 cm.

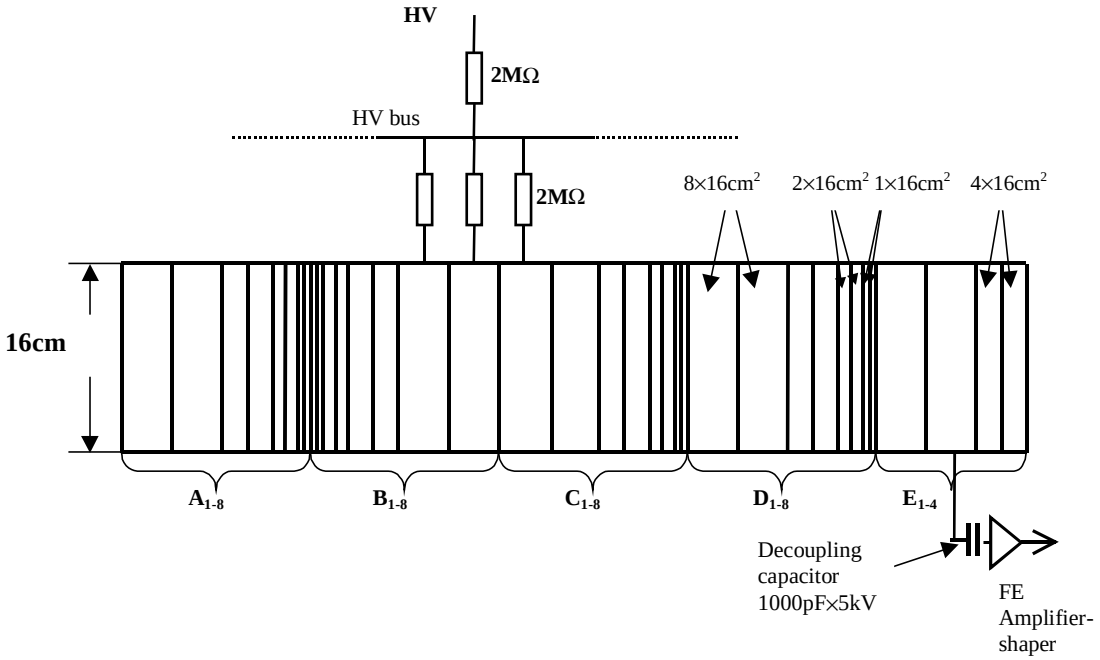

Fig.2. Wire pad structure in WPC-1.

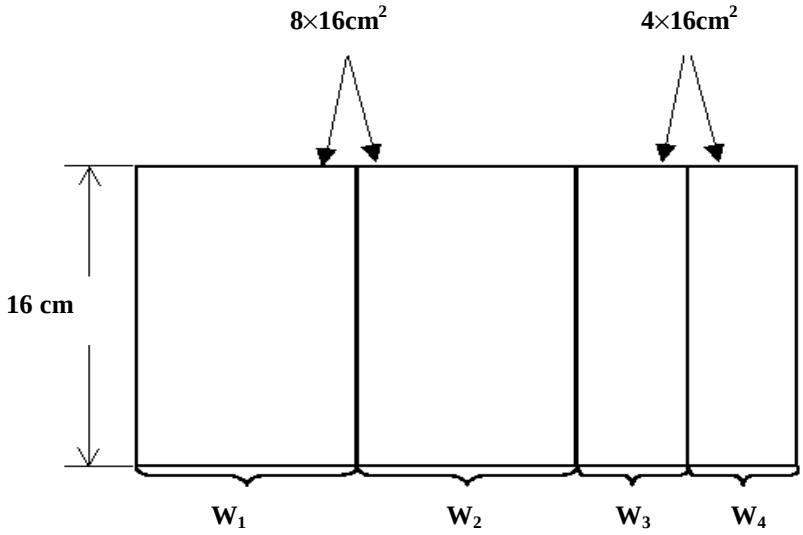

Fig.3. Wire pad structure in WPC-1M.

Two rows of Cathode pads:

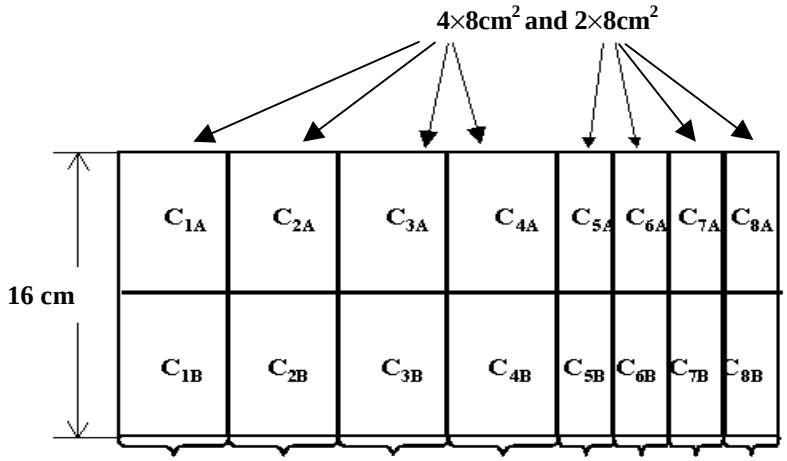

One row of Wire pads:

W1 W2 W3 W4 W5 W6 W7 W8

Fig.4. Wire and cathode pads in WPC-2.

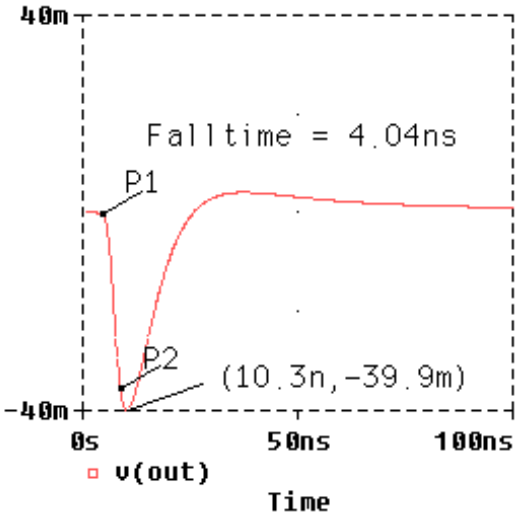

Fig.5*a*. Impulse response of the PNPI amplifier-shaper.
Fast channel.
SPICE calculations for Qo=8fC, Cdet=50pF.

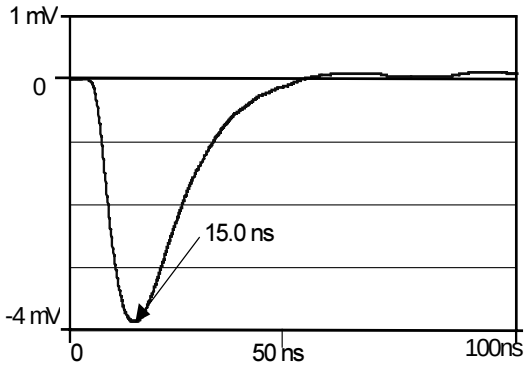

Fig.*5b.* Response to a signal with tail described by expression (1).
Fast channel.
SPICE calculations for Qo=8fC, Cdet=50pF.
T_{peak} *is shown with down arrow.*

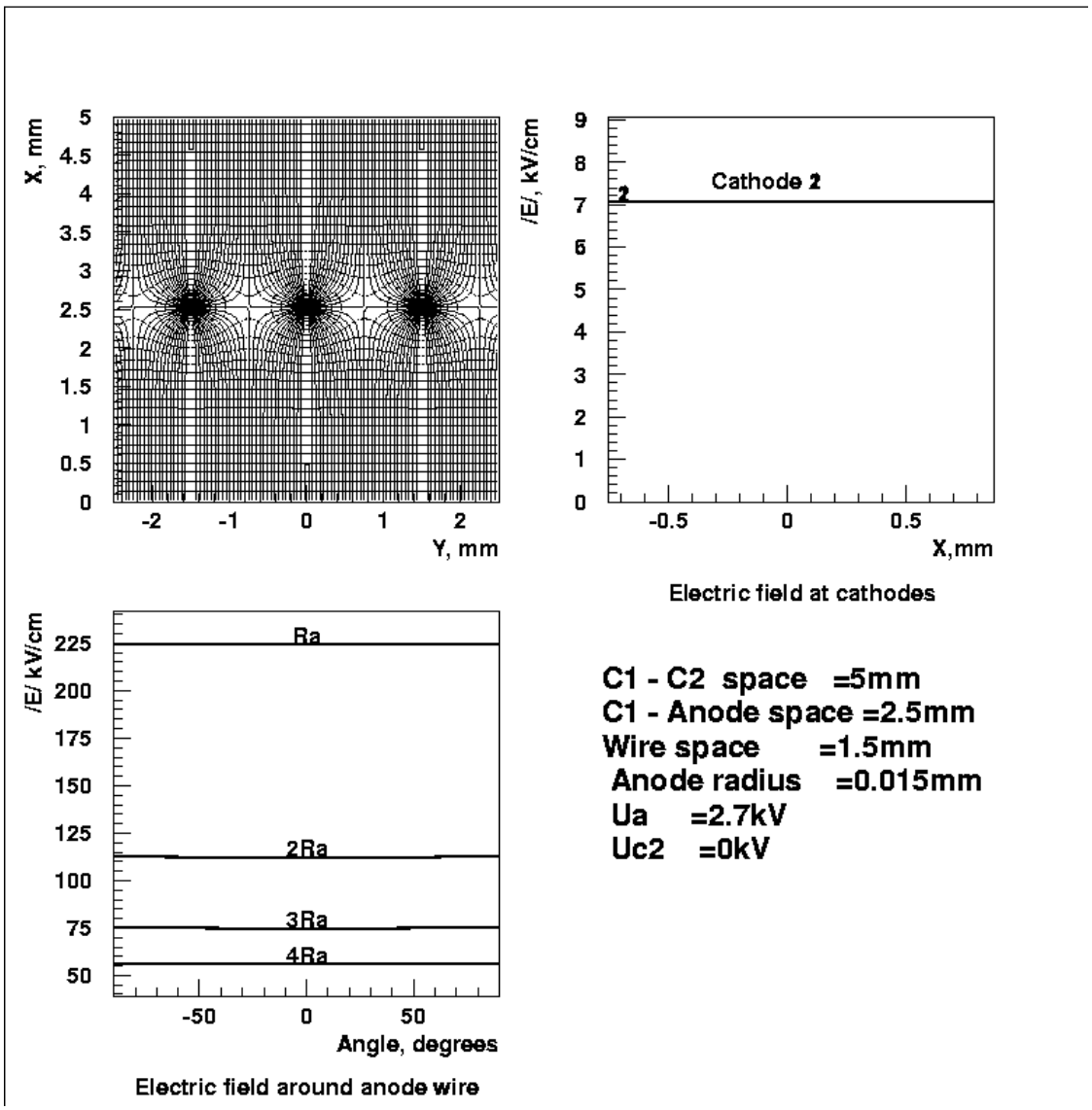

Fig.6. Electric field map in WPC.

a)

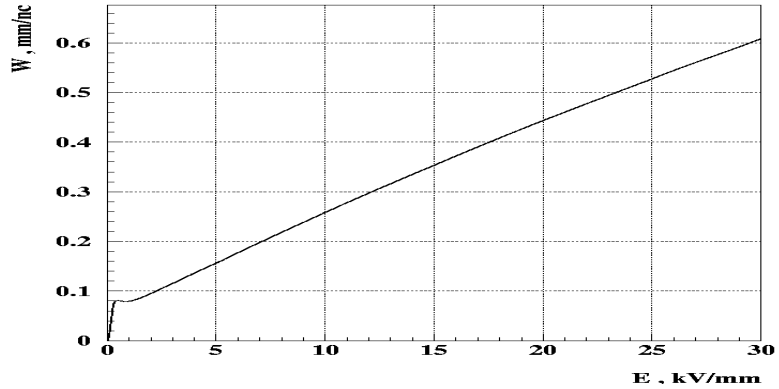

b)

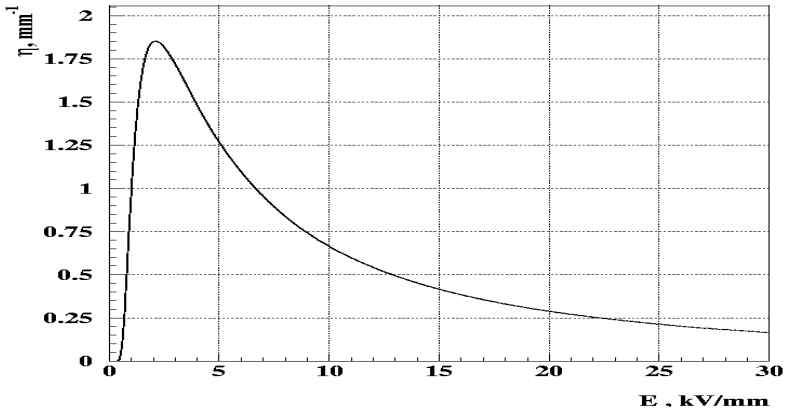

c)

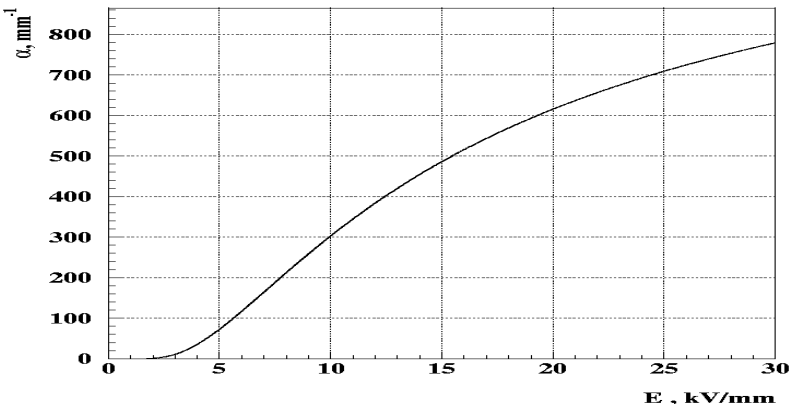

Fig.7. Electron drift velocity (*a*), electron attachment coefficient (*b*), and gas amplification factor (*c*) calculated with the Magboltz program for $Ar(60\%)+CO_2(30\%)+CF_4(10\%)$ gas mixture.
The gas amplification factor was multiplied by $K_\alpha = 0.7$ to achieve agreement with experiment.

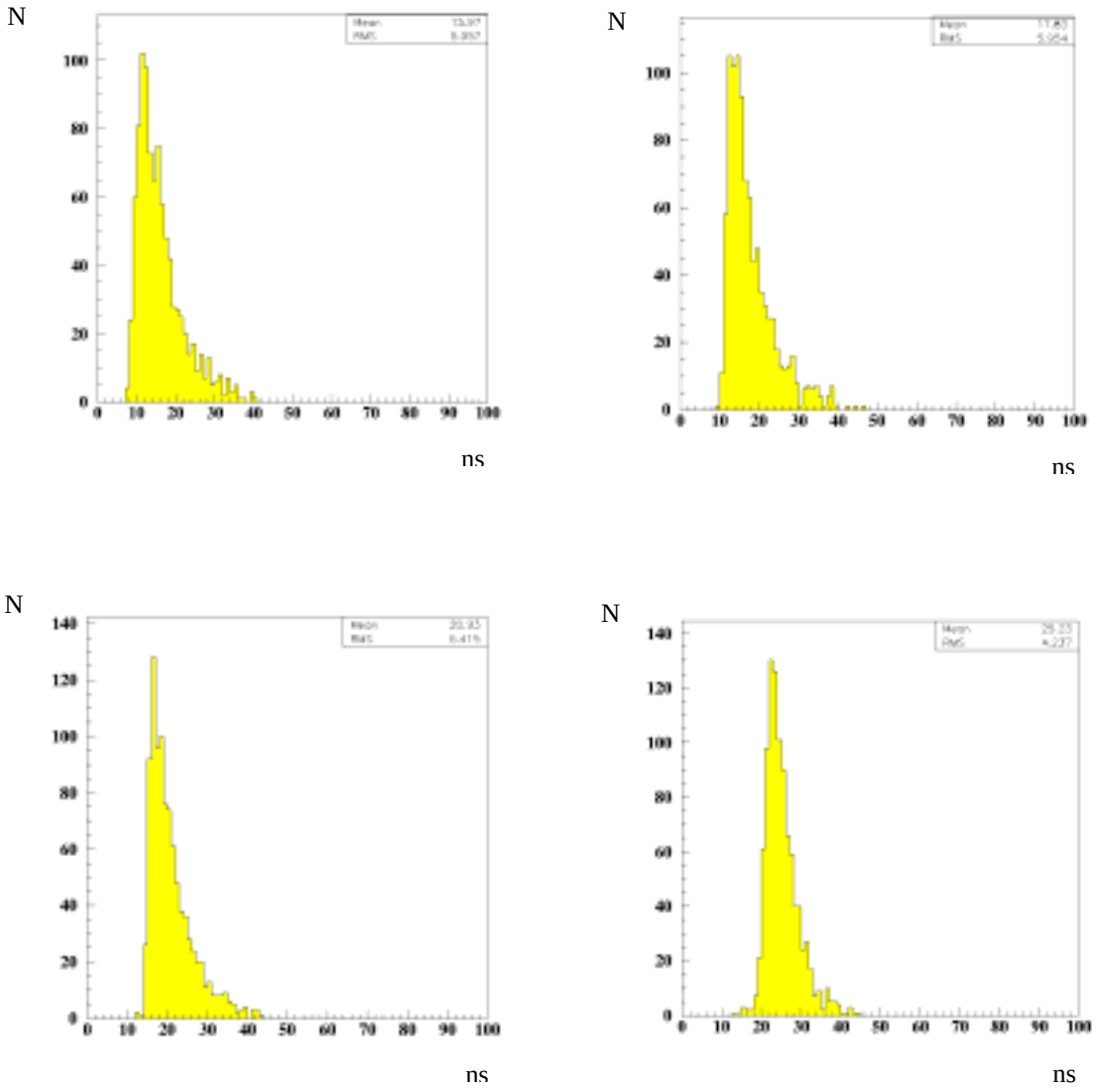

Fig.8. Calculated time distributions of signals from a single gap WPC for various distances of the particle trajectory from the anode wire
(t=0 corresponds to the particle entering time).
$\Theta = 0^O, \phi = 0^O$; Threshold = 30mV; Noise level = 4mV.

r.m.s., ns

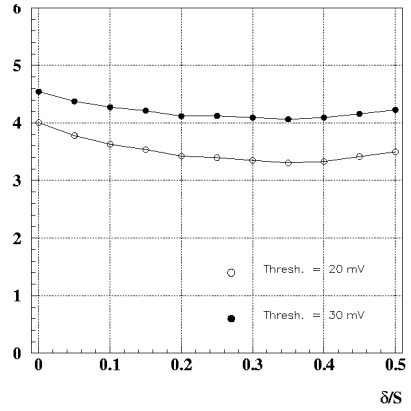

Ineff. (%) in 25 ns window

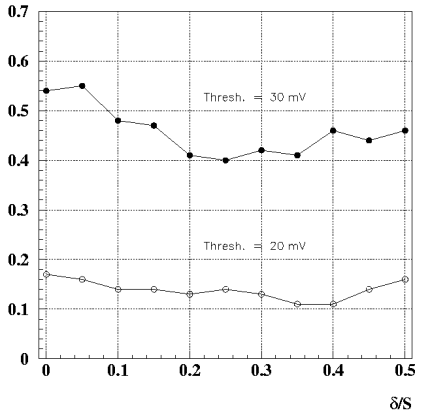

Ineff. (%) in 20 ns window

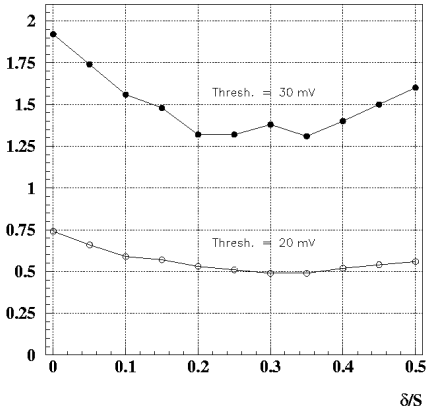

Fig.9. Calculated time resolution and inefficiencies of the double gap WPC for various staggering of the anode planes.
9GeV/c pions; $\Theta=\varphi=0^{\circ}$; Noise=4mV; Gas gain=1.2×10^{5}.

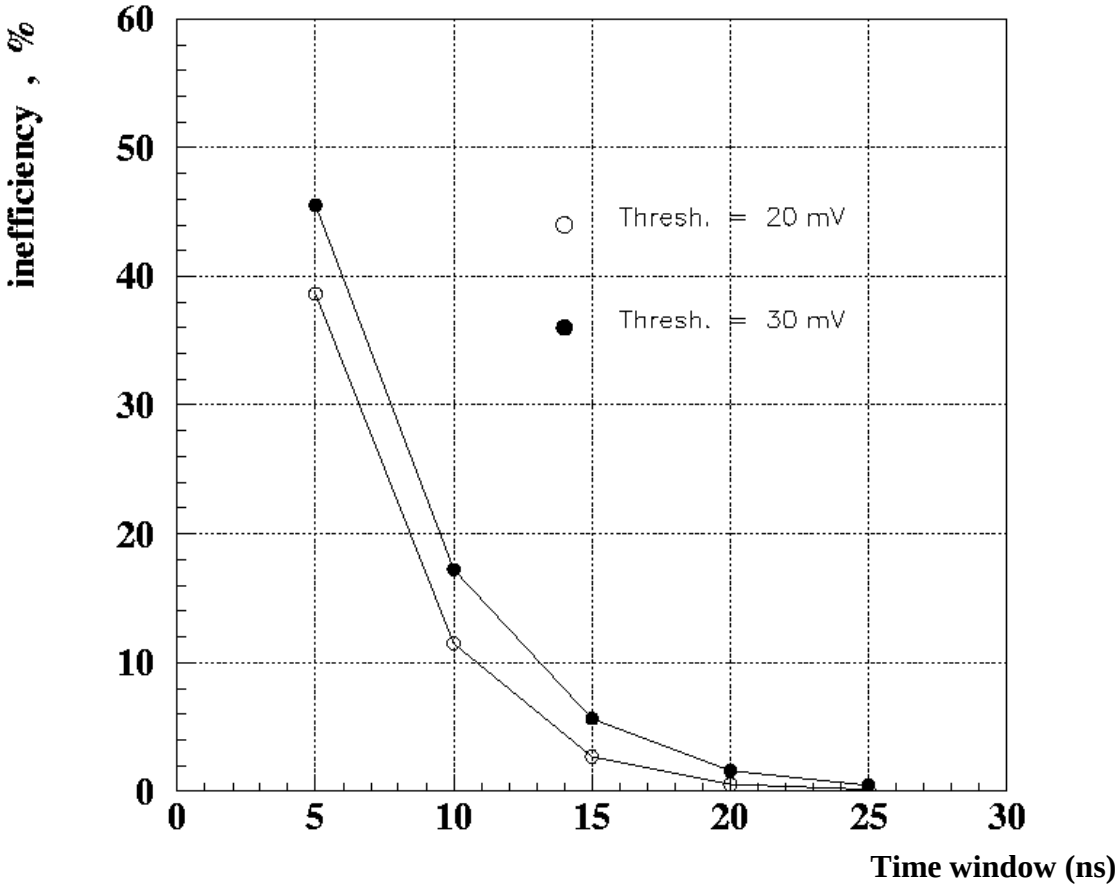

Fig.10. Calculated inefficiencies of the double gap WPC
for various time windows.
Staggering of the anode planes is $\delta/S=0.5$.
9GeV/c pions; $\Theta=\varphi=0°$; Noise=4mV; Gas gain=1.2×10^5.

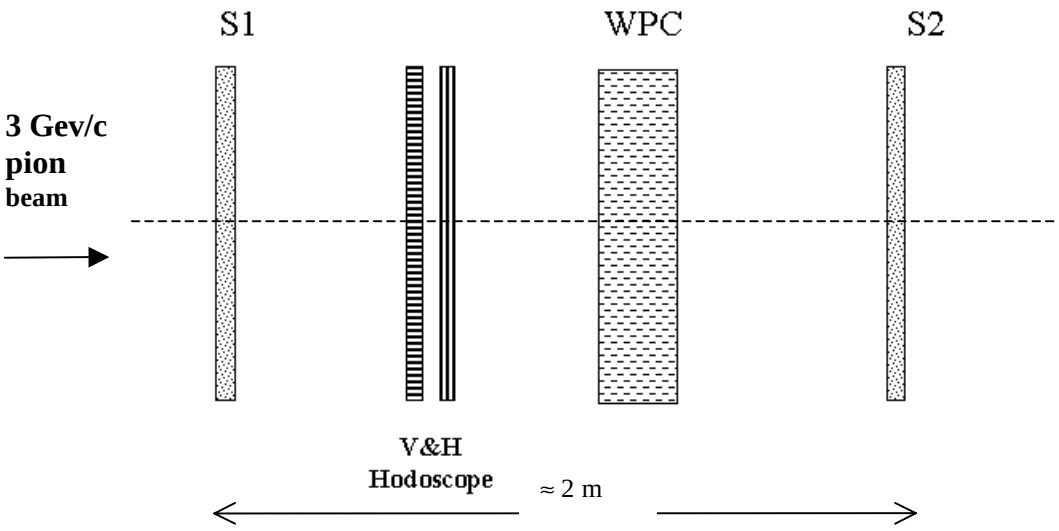

Fig.11. Experimental setup.

S1, S2 – scintillator counters of 15×15 cm^2 and 20×20 cm^2 size, respectively;
V&H Hodoscope – 8+8 scintillator counters of 1cm×8cm size each.

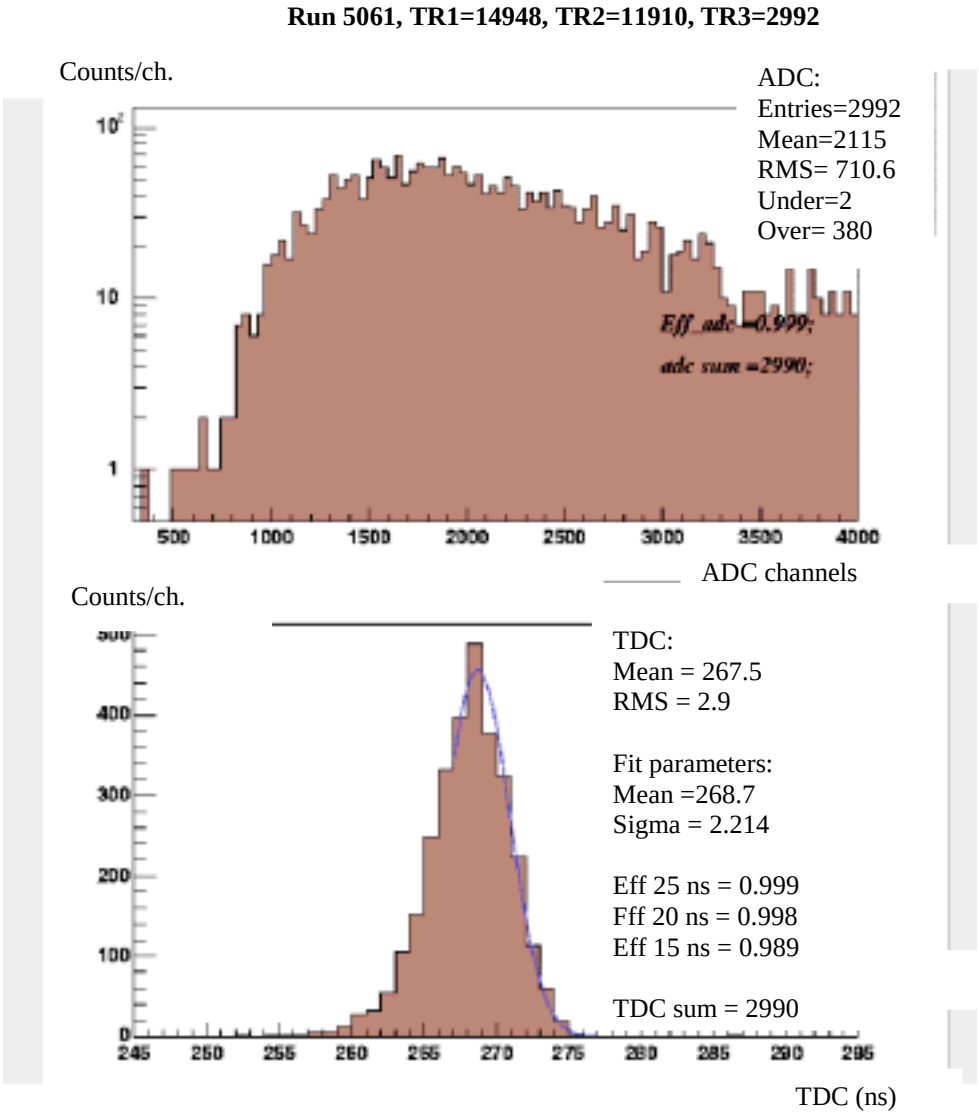

Fig.12. ADC and TDC spectra measured with WPC-2 prototype.

Ar(40%)+CO_2(45%)+ CF_4(15%) gas mixture;

HV=3.15kV; Thersh=20mV; Gas gain=2×10^5; ADC pedestal 250 ch.

Beam spot is inside the W3 wire pad. Pad size is 4×16 cm^2.

Eff_{ADC}=99.9% and Eff_{TDC} in various time windows were determined according to equations (5) and (6), respectively. The fit parameters correspond to the Gaussian fit of the initial part of the time distribution. The real time goes from the right to the left side of the plot.

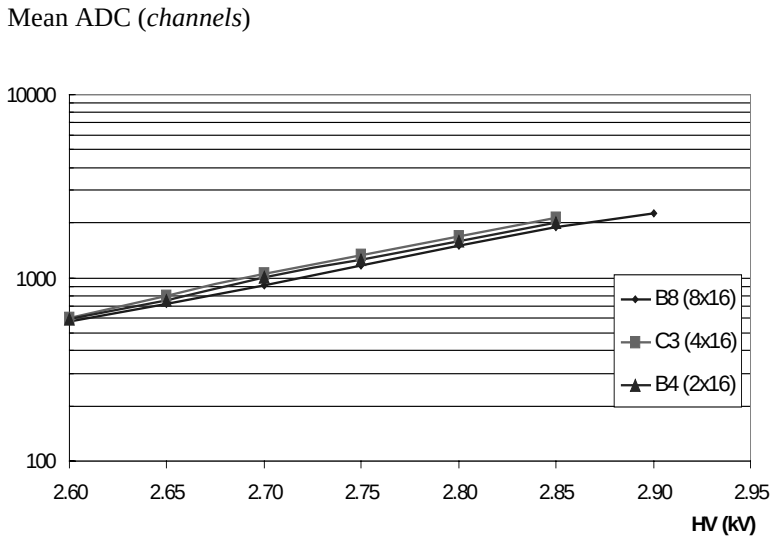

Fig.13. Mean values of ADC spectra vs HV.
Measurements performed with the gas mixture
$Ar(60\%)+CO_2(30\%)+CF_4(10\%)$ for various wire pads.
ADC pedestals are subtracted.
Gas gain =1.2×10^5 at HV = 2.7 kV.

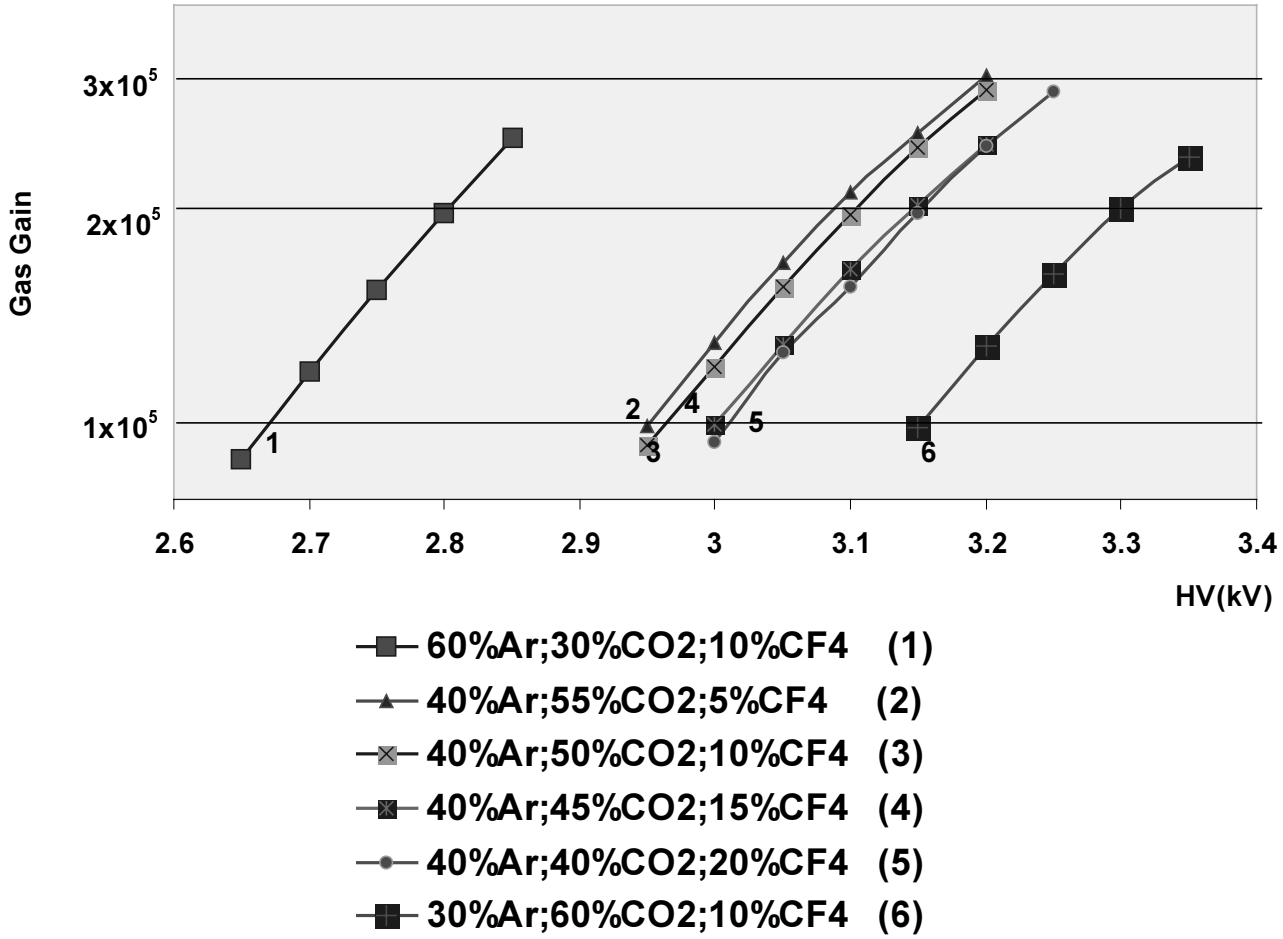

Fig.14. Gas gain vs HV for various $Ar/CO_2/CF_4$ gas mixtures.

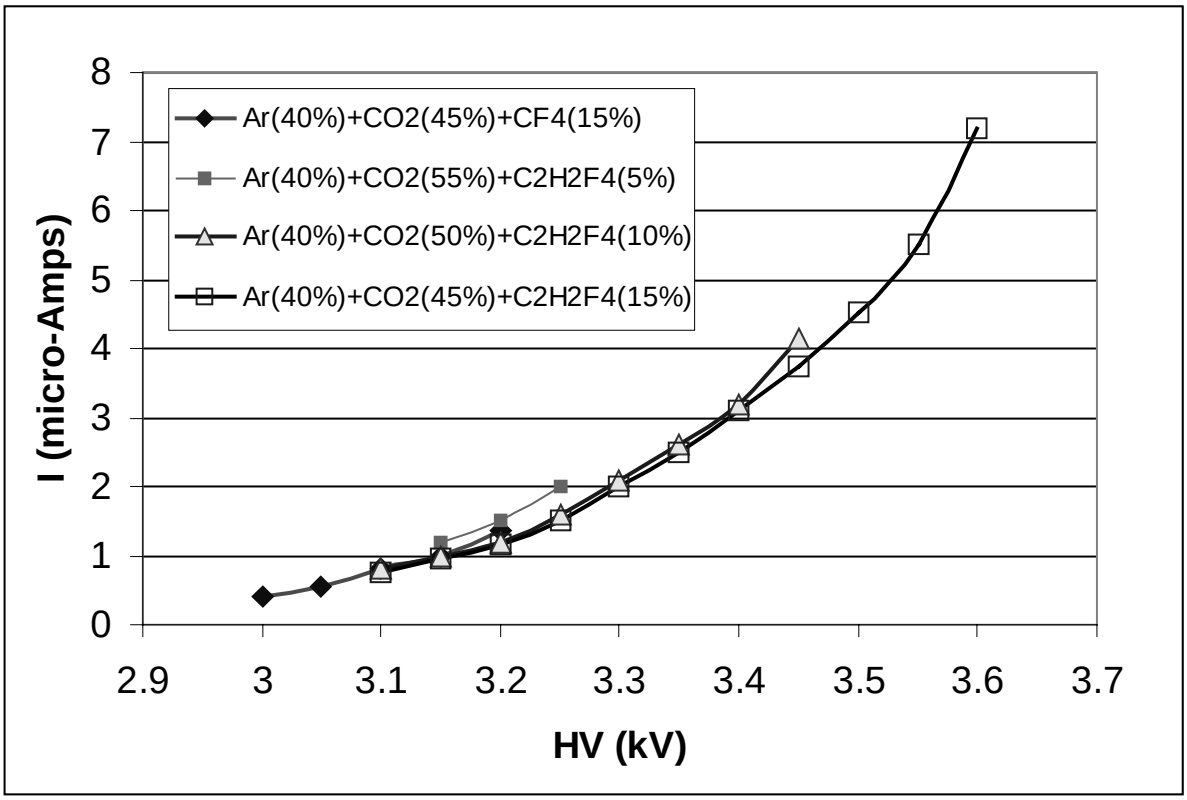

Fig.15. Beam induced current in WPC vs HV.
The current around 1μA corresponds to the gas gain of 2×10^5.

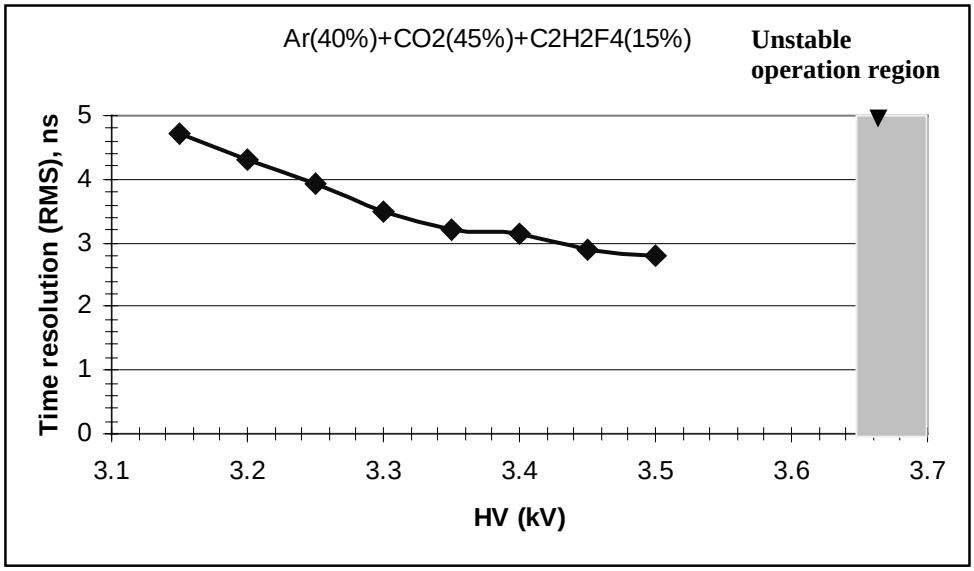

Fig.16. Time resolution of WPC with the Ar(40%)+CO_2(45%)+ $C_2H_2F_4$(15%) gas mixture vs high voltage.
WPC-1M prototype.
Threshold 20 mV; 8×16 cm^2 wire pad.
Beam spot is inside the pad size.
The plateau of better than 99% efficiency in 25 ns window extends from HV=3.2 kV to 3.6 kV.

RUN 5406, TR1=29922, TR2=20740, Tr3=2732

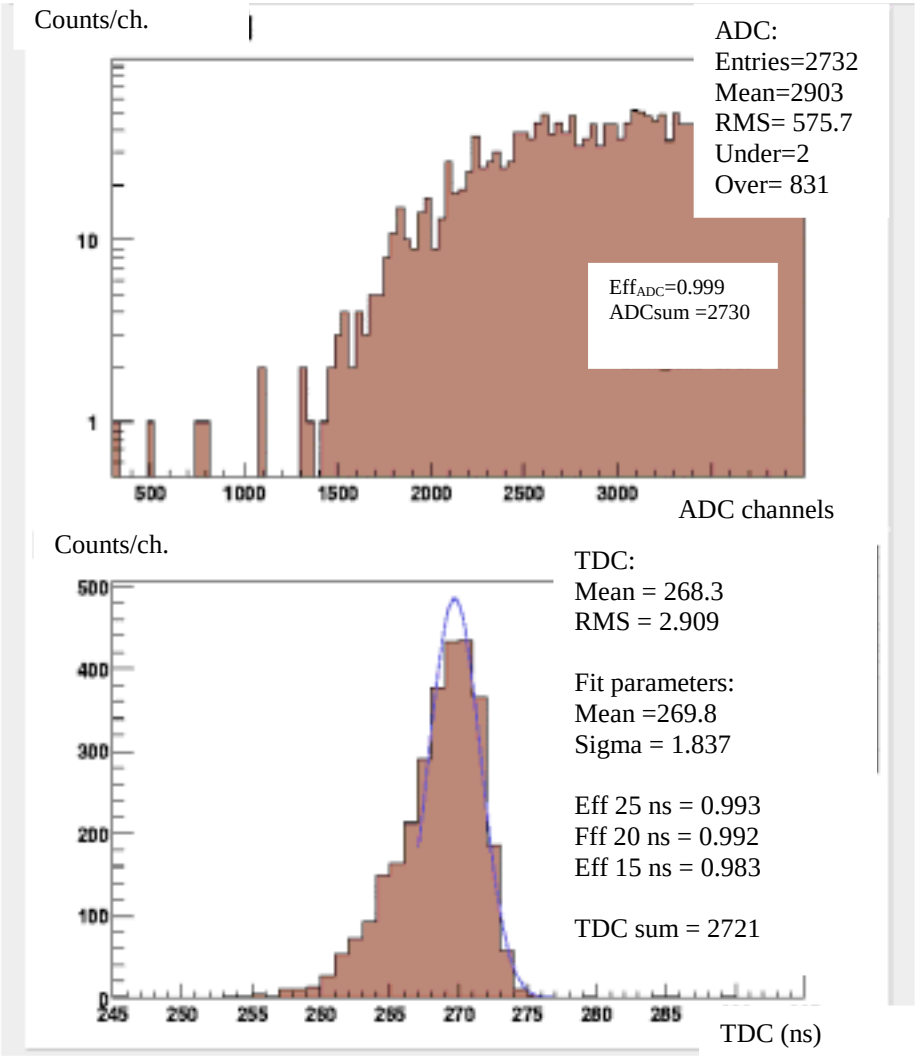

Fig.17. ADC and TDC spectra measured with WPC-1M prototype.
Ar(40%)+CO_2(45%)+ $C_2H_2F_4$(15%) gas mixture;
HV=3.45kV; Thersh=20mV.
Beam spot is inside the W2 wire pad. Pad size is 8×16 cm^2.

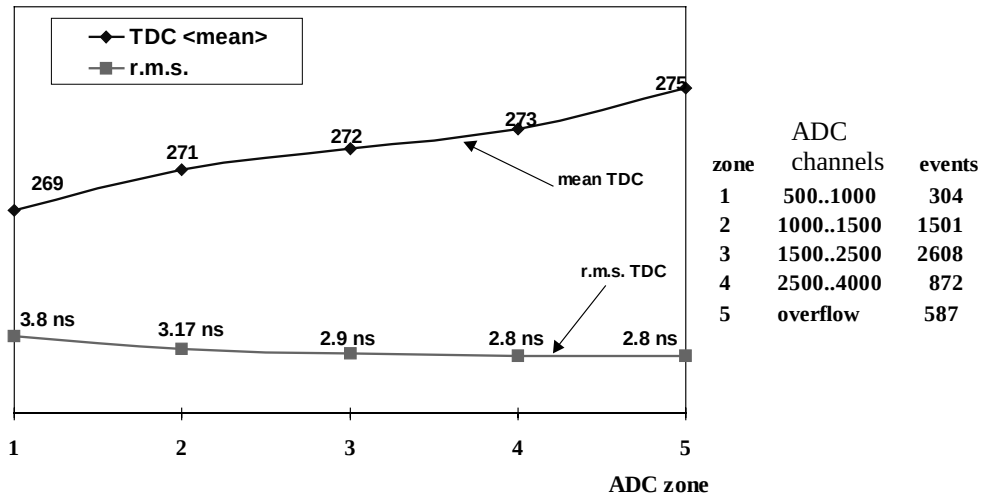

Fig.18. TDC mean and r.m.s. values vs ADC amplitude.
HV=3.15 kV. Ar(40%)+CO_2(50%)+CF_4(10%).

a)

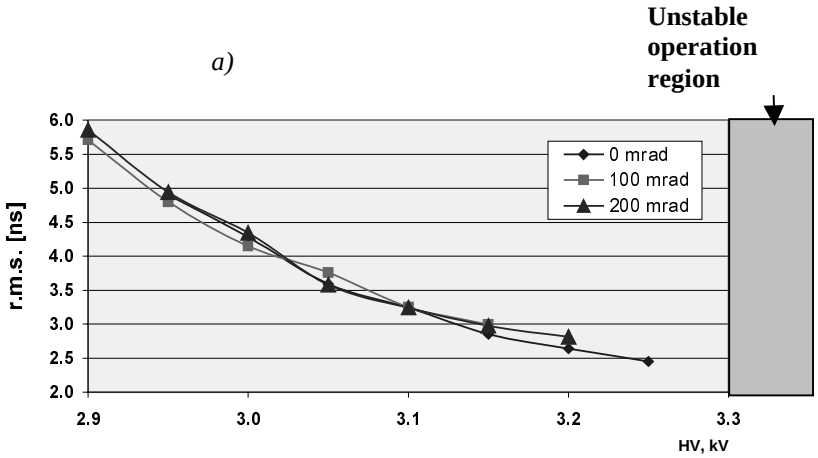

Pad size 4x16 cm^2; Ar(40%) + CO_2(50%) + CF_4(10%); Tresh=20 mV ;

b)

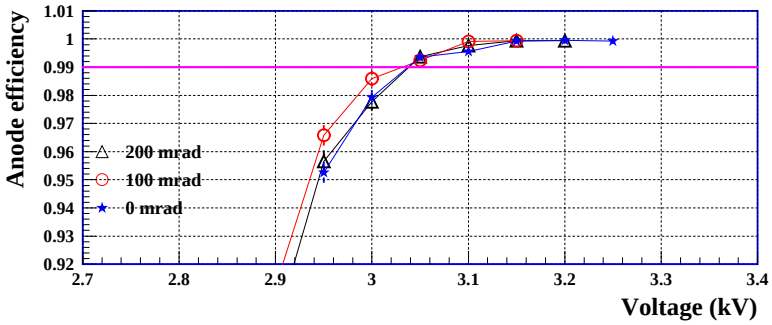

c)

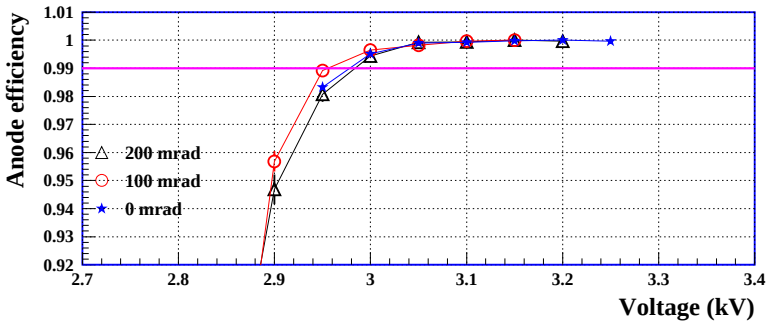

Fig.19. Time resolution (*a*), efficiency in 20 *ns* window (*b*), and efficiency in 25 *ns* window (*c*) vs HV measured with WPC-1 prototype for various Θ-angles.

Ar(40%)+CO_2(50%)+CF_4(10%); Threshold = 20 mV; Pad size 4×16 cm^2.

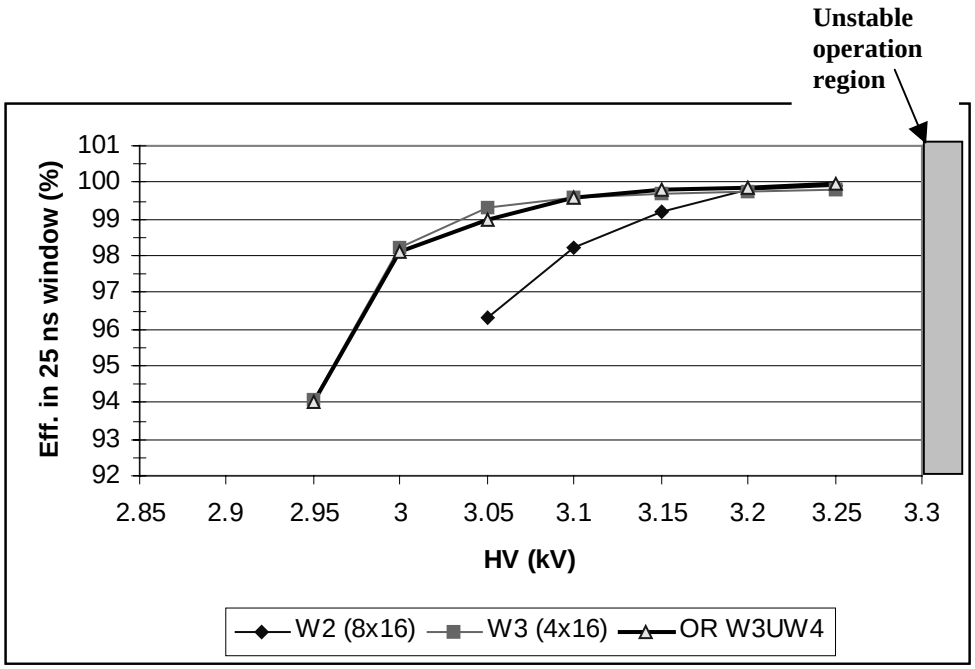

Fig.20. Comparison of efficiencies in 25 ns window for wire pads of various sizes in gas mixture Ar(40%)+CO_2(45%)+CF_4(15%). *WPC-1M prototype.*

The figure illustrates possibility to combine the wire pads in OR without deterioration the detection efficiency.

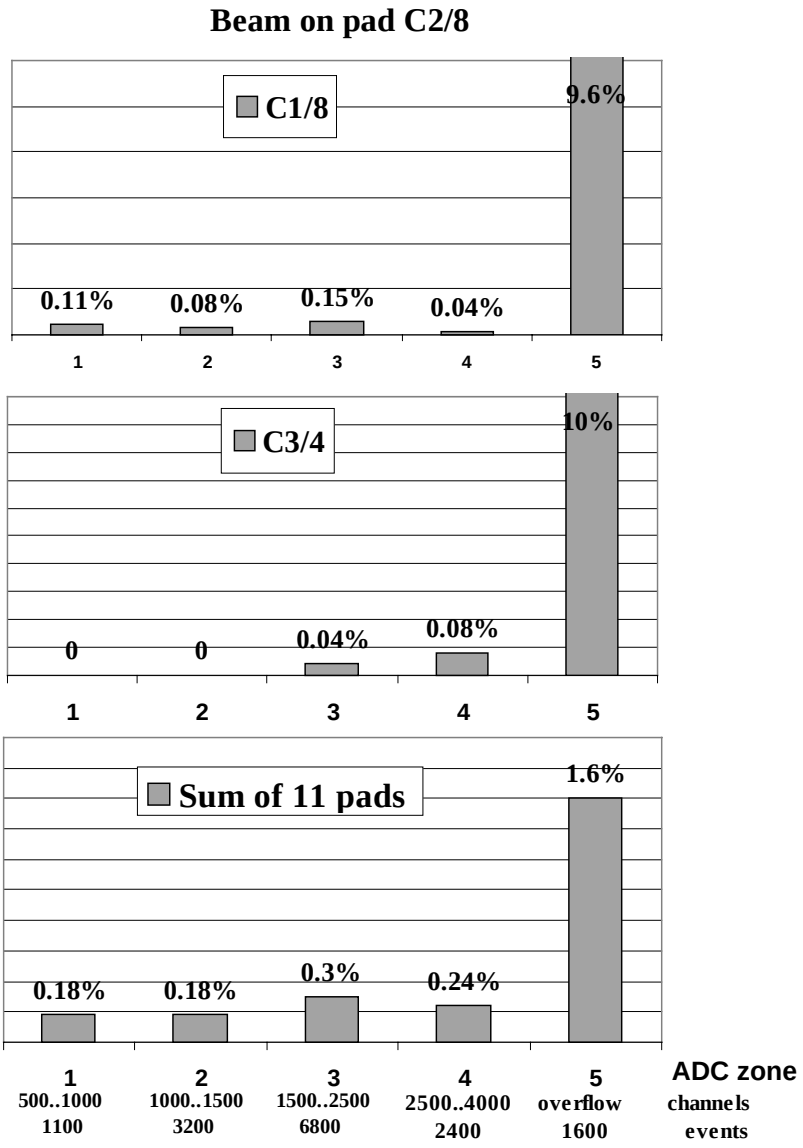

Fig.21. Cross-talks in TDC channels.
WPC-1M prototype.
The beam spot is inside wire pad W_{C2}.
Pad sequence: $W_{C1}(8\times16\ cm^2)\leftarrow W_{C2}(8\times16\ cm^2)\rightarrow W_{C3}(4\times16\ cm^2)$.
Gas gain 2×10^5; Threshold 20 mV.

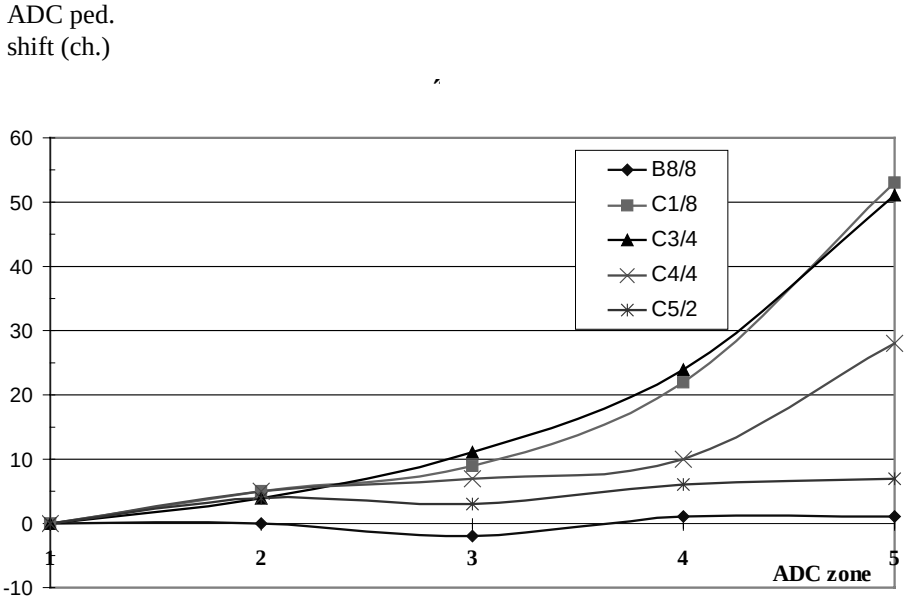

Fig.22. Cross-talk shift of ADC pedestals.

ADC zones correspond to ADC channels:

1	*500..1000*
2	*1000..1500*
3	*1500..2500*
4	*500..4000*
5	*ADC overflow*

WPC-1M prototype. The beam spot is inside wire pad W_{C2}.

Pad sequence:

$W_{B8}(8\times16\ cm^2) \leftarrow W_{C1}(8\times16\ cm^2) \leftarrow W_{C2}(4\times16\ cm^2) \rightarrow W_{C3}(4\times16\ cm^2) \rightarrow W_{C4}(4\times16\ cm^2) \rightarrow W_{C5}(2\times16\ cm^2$.